International Symposium on Niobium Microalloyed Sheet Steel for Automotive Application
Edited by S. Hashimoto, S. Jansto, H. Mohrbacher, and F. Siciliano
TMS (The Minerals, Metals & Materials Society), 2006

NIOBIUM MICROALLOYED CMnAlSiP TRIP STEEL

B.C. De Cooman and D. Krizan

Laboratory for Iron and Steelmaking
Department of Metallurgy and Materials Science
Ghent University
Technologiepark 903, 9052 Ghent, Belgium

Introduction

The first observation of an unexpected increase in formability, due to the austenite to martensite transformation in Fe-Ni alloys, was observed in 1937 by Wassermann [1]. In 1967 Zackay *et al.* [2] described how a phase transformation in highly-alloyed homogeneous metastable austenitic steels was the reason for the ductility enhancement. This effect of Strain-Induced Martensite (SIMT) leads to TRansformation Induced Plasticity, usually abbreviated as TRIP. Researchers at Nippon Steel Corporation showed that austenite stabilization also occurred during an isothermal bainitic transformation (IBT), a process often referred as "austempering", which followed an intercritical $\alpha+\gamma$ annealing of low alloy Si-bearing medium-C (0.12 - 0.55 %) CMn steel [3-6]. In this new class of low-alloyed TRIP steels the austenite is present as a disperse phase. Since C hardening is much higher for the martensite than for the austenite phase and the volume expansion due to this transformation results in plastic deformation and work hardening of the surrounding ferrite, a localized strengthening is obtained. These effects postpone further deformation in this area and move the martensitic transformation to neighbouring areas (see Figure 1), leading to a delay in the onset of macroscopic necking and consequently, to higher values of uniform and total elongation.

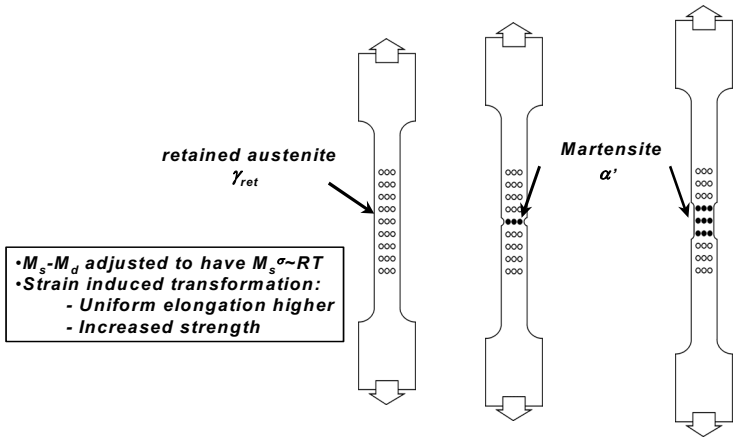

Figure 1. Schematic explanation of the TRIP effect showing that the retained austenite transforms into martensite when the stress is applied and the martensitic transformation occurs in neighboring areas in sequence to disperse strain.

Two factors determine the TRIP effect, causing enhancement of mechanical properties of TRIP steels: the volume fraction and the stability of the retained austenite. The optimal volume fraction of retained austenite for a significant TRIP effect to occur is reported to be in the range

of 10-20 vol. %. Moreover, the volume fraction of retained austenite directly determines the C content and grain size of the retained austenite, its two main stabilization factors. The stability of the retained austenite dictates when the SIMT occurs during straining of TRIP high strength steel. Unstable retained austenite transforms almost immediately upon deformation, increasing work hardening rate and formability during the stamping process. At the appropriate stability of the retained austenite, the SIMT begins only at strain levels beyond those produced during stamping and forming, and the retained austenite is still present in the final part; it can transform into martensite in the event of a crash, providing greater crash energy absorption. If the retained austenite is too stable, the SIMT may start beyond the uniform elongation. In this case, no additional work hardening is expected and this delayed TRIP effect will not contribute to the enhancement of mechanical properties. The stability of the retained austenite depends on a number of stabilization factors:

The C content: The C content lowers the M_s temperature and therefore stabilizes retained austenite. The optimal C content in the retained austenite has to be in the range of 0.5-1.8 wt. % in order to provide the desirable TRIP effect.

The size of the retained austenite islands: The M_s temperature of the retained austenite is above room temperature. Smaller austenite particles contain less potential nucleation sites for transformation to martensite and consequently require a greater total driving force for the nucleation of martensite. This will lower the M_s temperature to below room temperature (Figure 2). It has been suggested that the grain size of the retained austenite must be in the range of 0.01 μm to 1 μm to ensure the TRIP effect in low- alloyed multiphase TRIP steels. Larger retained austenite particles may already be partially transformed into martensite or transform into the martensite at the early stages of straining. Particles smaller than 0.01 μm do not undergo the strain-induced transformation. The stabilization of retained austenite due to the smaller grain size can also be explained by the size of the strain induced martensite formed, Figure 3. If the same volume fraction of retained austenite is considered for large and small retained austenite grains with the same volume density of the potential nuclei available for the strain-induced martensite transformation. The activation of the martensitic nuclei in the case of the smaller retained austenite grain will lead to a formation of the less martensite than in the case of the larger retained austenite grains, i.e. the transformation kinetics are reduced for smaller austenite particles.

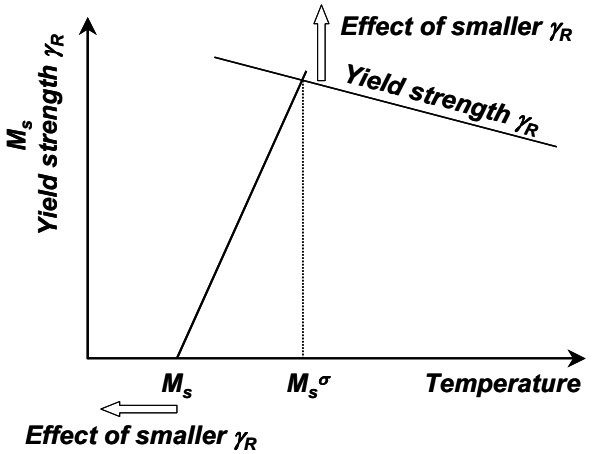

Figure 2. Effect of a smaller grain size of retained austenite on its stability.

The volume fraction of the retained austenite: As mentioned in the previous paragraph, the optimal volume fraction of retained austenite for a pronounced TRIP effect is reported to be in the range of 10 - 20 vol. %. Smaller amounts of retained austenite cannot ensure a significant TRIP effect, since the C content may then be too high to result in strain-induced formation of

martensite. Large amounts of retained austenite have a low C content, leading to a low stability of the retained austenite;

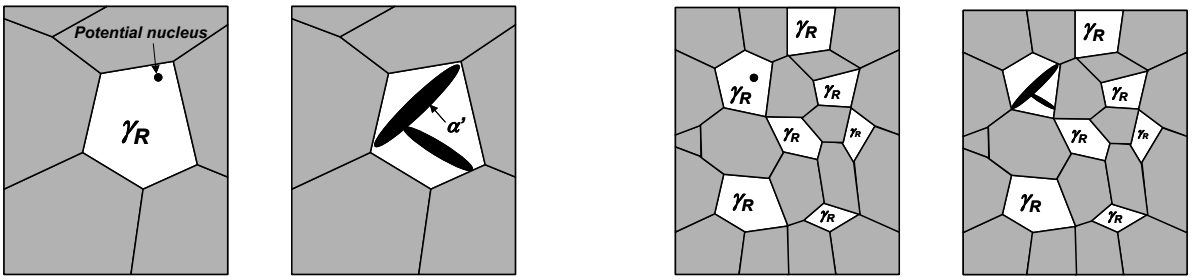

Figure 3. Schematic explanation of a decrease of the volume fraction of strain induced martensite due to a smaller grain size of retained austenite; less martensite is formed for the same density of martensite nuclei and amount of retained austenite, when the retained austenite grains are smaller (right).

The stress-state: As a result of the volume change associated with the transformation, the stability of retained austenite is stress state dependent; it is highest for uniaxial compression and lowest for plane strain conditions.
Morphology and distribution of retained austenite in the microstructure: the retained austenite can be classified in two groups: (1) isolated retained austenite islands in a soft ferrite matrix adjacent to bainite and possibly martensite and (2) thin films of retained austenite along the martensite or bainite lath boundaries, or blocky retained austenite in these hard second phases. In group (2), a higher hydrostatic pressure, resulting from the surrounding hard phase, constrains a higher volume expansion and shear deformation provoked by the strain-induced martensite transformation more than in the retained austenite of group (1).
Precipitation: The possible precipitation strengthening of the surrounding phases increases the resulting hydrostatic pressure, which is in turn associated with a higher stability of retained austenite. It has been also reported that the precipitates formed in retained austenite increase its yield strength, and lower its stability due to an increase of the M_s^{σ} temperature, causing a shift of the stress-assisted martensite formation closer to the ambient temperature. On the other hand, an increase of the yield strength of retained austenite may also cause its stabilization due to a decrease of the autocatalytic formation of strain-induced martensite. Precipitates formed in retained austenite hinder the strain-induced martensite propagation, which causes its stabilization.
ISFE: A low ISFE results in a larger distance between the Shockley partial dislocations. For lower ISFE of austenite, the SIMT becomes more favorable as the primary shear required for the transformation requires a similar type of partial dislocations.

Development of Cold Rolled Hot Dip Galvanized TRIP Steels

Figure 4 shows the summary of the development of low C cold rolled TRIP steels. Current low alloy TRIP steels are characterized by a very low total content of alloying elements of about 3.5 wt. %. Conventional TRIP steel compositions are usually based on the original 0.12-0.55 wt. % C, 0.2-2.5 wt. % Mn, 0.4-1.8 wt. % Si concept proposed by Matsumura. Further studies have however revealed important difficulties in hot dip galvanizing of high Si cold rolled TRIP steels. Si is also known to cause a low ductility level in the as-cast condition and it leads to an increase of the ductile-to-brittle transition temperature. These are the main reasons to keep the Si content low. This can be achieved by a partial or full substitution of Si by elements with similar properties. It is known that Al and P, in addition to being strong ferrite stabilizers, effectively inhibit the formation of cementite [7-12]. In the present study the CMnAlSiP alloy concept was

therefore chosen to achieve a reference TRIP steel with a high tensile strength level in combination with a good elongation: tensile strength up to 900 MPa and total elongation of about 28 %. The C content was to be kept low (≤ 0.25 wt. %) for reasons of weldability. One of the ways to increase the strength of CMnAlSiP TRIP steels, without deteriorating their weldability, is the addition of micro-alloying elements, such as Nb or Ti. By doing so, a tensile strength level above 980 MPa, combined with good formability properties, i.e. an elongation of 22 %, can be achieved. A combination of micro-alloying elements such as Nb+V and Ti+V can even result in an additional increase in strength up to 1040 MPa at appropriate formability properties, an elongation of 20 %.

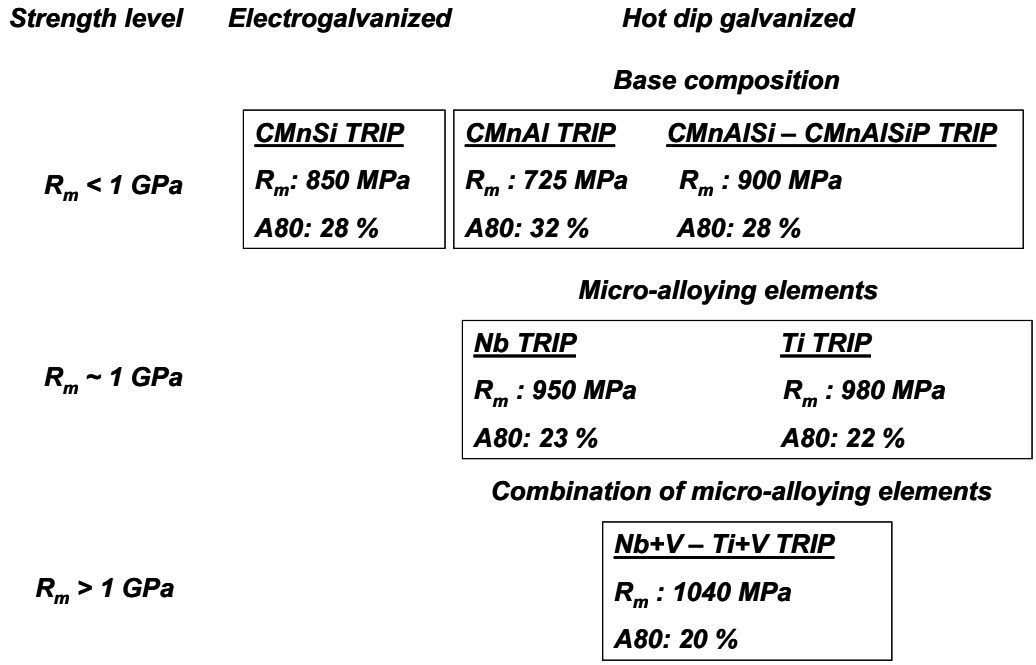

Figure 4. Development of low C multi-phase cold rolled TRIP steel.

Microalloying Concept in TRIP Steels

The role of micro-alloying elements in standard Nb HSLA steel has been thoroughly investigated in the past. The study of micro-alloyed TRIP steels started more recently and is of higher complexity compared to standard HSLA steels. The main differences are as follows [13-18]:

The C content: The C content of TRIP steels (~ 0.25 wt. %) is higher than in HSLA steels (< 0.1 wt. %). This accelerates the kinetics of the carbide or carbo-nitride precipitation during the various processing stages of micro-alloyed TRIP steels. Moreover, the higher C content of TRIP steels lowers the solubility of the carbides and carbo-nitrides of micro-alloying elements compared to the HSLA steels. This effect is more pronounced in the case of the Nb micro-alloyed TRIP steels as shown in Figure 5.

The number of phases: Whereas HSLA steels deal with the precipitation in a single-phase microstructure (ferrite), the precipitation in micro-alloyed TRIP steels occurs in a complex microstructure containing polygonal ferrite, bainitic ferrite and retained austenite.

Strength level: While the tensile strength level of HSLA is usually less than 600 MPa, the strength of micro-alloyed TRIP steels may exceed 1 GPa.

Plastic behavior: In HSLA steel, the dislocations are immobilized by Nb(C,N) precipitates acting as obstacles during straining. In micro-alloyed TRIP steels transformation strengthening is an additional hardening mechanism.

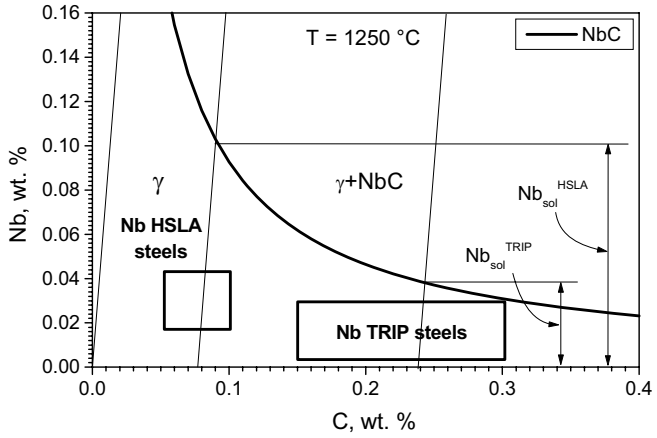

Figure 5. Increased carbide formation in TRIP steels compared to HSLA steels. (T: 1250 °C).

Processing of Nb micro-alloyed TRIP steels

The micro-alloyed TRIP steels go through a more complex metallurgy during their processing compared to standard TRIP steels. The formation of precipitates of micro-alloying elements influences the static recrystallization, phase transformations, volume fraction and size of present phases.

Hot rolling

A schematic representation of the hot rolling process for the Nb micro-alloyed TRIP steel is shown in Figure 6.

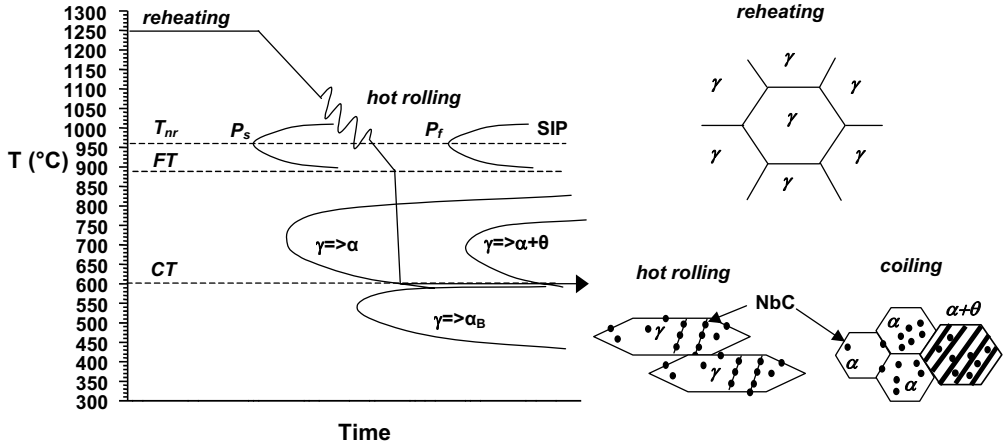

Figure 6. Schematic representation of hot rolling schedule and possible precipitation stages in the Nb micro-alloyed TRIP steel: T_{nr} – non-recrystallization temperature, *FT*- finishing temperature, *CT* – coiling temperature, SIP – strain-induced precipitation, P_s – precipitation start, P_f – precipitation finish, α - ferrite, γ – austenite, θ – cementite.

The dissolution of the primary NbC and/or Nb(C,N) precipitates formed during the casting of micro-alloyed TRIP steel is expected to take place during reheating. NbC or Nb(C, N) particles usually form by strain-induced precipitation (SIP) during hot rolling. They retard the static recrystallization of the deformed austenite and hence give rise to the strain-accumulation and pancaking of the austenite grains. The ferrite grain, obtained after the allotropic transformation of a pancaked austenite, is much smaller than obtained when the successive hot rolling passes are carried out at temperatures higher than the SRX temperature. The temperature, below which

pancaking occurs due to the absence of interpass static recrystallization, is defined as the non-recrystallization temperature T_{nr}. NbC and Nb(C,N) may also be formed during the austenite to ferrite transformation by the transformation-induced precipitation (TIP) mechanism, mainly caused by the C-enrichment at the transformation boundary and the lower solubility of the carbides and carbo-nitrides in ferrite. These precipitates effectively contribute to the further strengthening of the steel.

Annealing stage

After hot rolling and coiling, the steel is cold rolled and annealed in order to obtain its TRIP characteristics. A schematic representation of the heat treatment, the evolution of the C content in the austenite and possible precipitation is shown in Figure 7. The initial microstructure before intercritical annealing (IA) consists of cold rolled ferrite and pearlite, the latter containing some 0.8 wt. % C. In the initial stage of IA, pearlite transforms into austenite. The C content of the intercritical austenite then gradually decreases to approximately 0.3 – 0.4 wt. %. A sufficiently high intercritical annealing temperature (T_{IA}) may result in the dissolution or further growth of NbC or Nb(C,N) precipitates already formed in the previous processing stages. After IA the steel is cooled to the isothermal bainitic transformation temperature (T_{IBT}). The cooling rate between IA and IBT stage must be higher than 15 °C/s in order to avoid the formation of pro-eutectoid ferrite. For this reason, the TIP in this stage is also suppressed. The subsequent IBT results in a further C enrichment of the remaining austenite to about 1.5 wt.%. The NbC or Nb(C,N) precipitation is not expected during the IBT due to the insufficient diffusivity of Nb at that temperature. The final microstructure consists of ferrite, bainite and retained austenite.

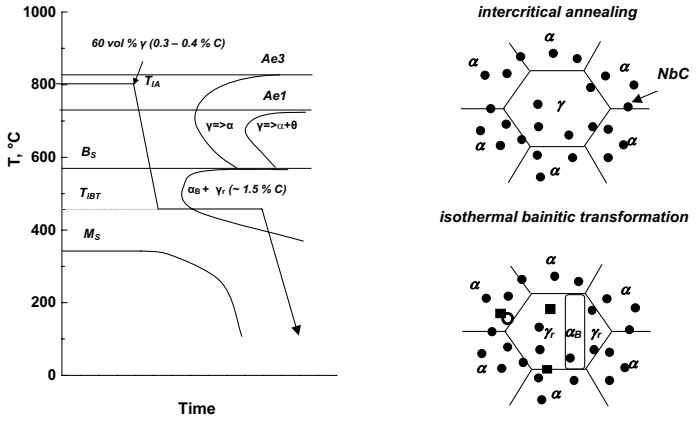

Figure 7. Thermal cycle and TTT – diagram of the intercritical austenite phase (left); Evolution of the C content of the austenite and precipitation of NbC in the micro-alloyed TRIP steel containing 0.25 %C (right): T_{IA} – intercritical annealing temperature, T_{IBT} – isothermal bainitic transformation temperature.

Experimental Procedure

The chemical composition of the laboratory cast steels used for the present work is shown in Table I. The reference material is a CMnAlSiP TRIP steel with a chemical composition as close as possible to that of the Nb micro-alloyed TRIP steel. The 100 kg vacuum cast steels were cut into blocks of 25 mm thickness. After reheating at 1250 °C for 1h, the blocks were subsequently hot rolled in 6 passes to 3 mm thickness. The finishing temperature and the coiling temperature were 880 °C and 600 °C, respectively. After hot rolling, the sheets were pickled and cold rolled to a final thickness of 1 mm. After cold rolling, longitudinal tensile test specimens with a width of 20 mm and a gauge length of 80 mm were machined. The tensile samples were then annealed

in salt baths using the two-step thermal cycle shown in Figure 8. After soaking at T_{IA} in the intercritical α+γ phase range, the samples were quenched in a second salt bath and held at T_{IBT}. T_{IA} was chosen on the basis of Thermo-calc calculations. An equilibrium phase distribution of 60 % ferrite and 40 % austenite was aimed for at the intercritical temperature. This phase composition is obtained at about 800 °C (Figure 9). Two T_{IA} temperatures, 770 °C and 800 °C, were chosen in order to evaluate the influence of the T_{IA} on the mechanical properties of the investigated steels.

Table I. Chemical composition (wt. %) of laboratory TRIP steels.

	C	Mn	Si	Al	P	Nb	N
Reference	0.22	1.50	0.44	1.34	0.073	-	0.0045
Nb micro-alloyed	0.25	1.67	0.45	1.38	0.080	0.081	0.0065

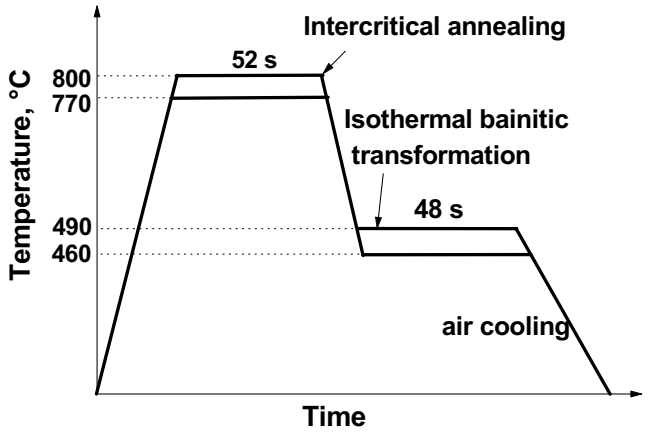

Figure 8. Schematic of the thermal cycle used to obtain a cold rolled TRIP steel.

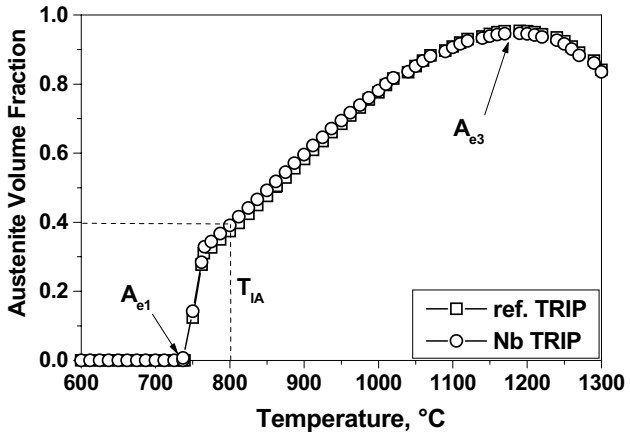

Figure 9. Calculated equilibrium austenite volume fraction as a function of the temperature.

Two different T_{IBT} temperatures were chosen to simulate the bainite transformation in continuous galvanizing lines. A T_{IBT} of 460 °C corresponds to the temperature of the Zn bath whereas the temperature of 490 °C reflects the maximum strip temperature of the sheet prior to entering the Zn bath. The microstructure of the TRIP steels investigated was examined by light optical microscopy (LOM) after LePera etching. In this etching technique, ferrite is coloured blue or orange, bainite is dark and the martensite/austenite phase is white. A double etching technique was applied to determine the size of the retained austenite particles. At first, the samples were immersed in a 10 % aqueous Na_2SO_5 for 10 s and afterwards in Klemm's reagent for 60 – 90 s. Using this etching technique, retained austenite appears as white while all other phases are dark.

The volume fraction of the ferrite, bainite and retained austenite/martensite particles was determined on 15 LePera etched micrographs per steels grade by means of image analysis. Microstructural observations were made by scanning electron microscopy (SEM) and transmission electron microscopy (TEM) using thin foils. TEM was used for the observation and the characterization of the precipitates present in the steel. The precipitates were identified by Selected Area Diffraction Patterns (SADP). The size of precipitates was defined as the average length of the precipitate measured in two perpendicular directions. The size of about 500 precipitates was determined separately in ferrite and austenite in the cold rolled condition. An equilibrium model and single particle kinetic model were used to determine the volume fraction and the size of the precipitates theoretically. The volume fraction of retained austenite, V_γ, was determined by X-ray Diffraction (XRD) on a diffractometer using Mo K_α radiation. The Direct Comparison Method was used with the integrated intensity of the $(200)_\alpha$, $(211)_\alpha$, $(220)_\gamma$ and $(311)_\gamma$ peaks. In addition, the C content of retained austenite, in mass-%, was calculated using [19]:

$$C_\gamma=(a_\gamma - 0.3570)/3.8\ 10^{-3}$$

where a_γ represents the lattice parameter of austenite in nm. In order to determine the exact volume fraction of retained austenite, which transformed into martensite during straining, i.e. the strain-induced transformation kinetics, interrupted tensile tests combined with XRD measurements were carried out. The measurements were performed up to 0.15 of true strain, i.e. well within the homogenous deformation range of the specimen. The mechanical properties were determined by tensile testing. The tensile test samples gauge length was 80 mm. The samples were machined with their length parallel to the rolling direction. The mechanical properties were characterized by means of the yield strength (R_e), the tensile strength (R_m), the uniform elongation (*UE*) and the total elongation (*TE*). The tensile test was also used to determine the M_s^σ temperature of the retained austenite by means of single specimen temperature variable tensile test (SS-TV-TT) method. The SS-TV-TT technique involved measuring the 0.2 % flow stress for a crosshead speed of 2.7 mm/min as a function of temperature. Starting at a relatively high temperature (~30 °C), the specimen was strained up to the 0.2 % flow stress and a small additional prestrain (0.5 %) was given to remove the yield point elongation due to the unpinning of dislocations in the soft ferrite phase. The sample was then unloaded and the temperature was lowered by 10 °C. The procedure was repeated in a temperature step of 2°C till –20 °C. The M_s^σ temperature is determined as the transition from continuous to discontinuous yielding.

Results

Hot rolling

Figure 10 shows the results of the equilibrium model calculation for the precipitation state in the case of the Nb micro-alloyed TRIP steel. The precipitation of pure NbC is expected to take place during the processing of the Nb micro-alloyed TRIP steel. The calculated dissolution temperature of NbC is 1410 °C, which means that 420 ppm of Nb is tied up as NbC after reheating. Thus, the amount of Nb available for the precipitation of NbC during further processing is 390 ppm. The NbC precipitation is completed at 700 °C. The model calculations and experimentally determined precipitated Nb fraction after reheating and processing are compared in Figure 11.

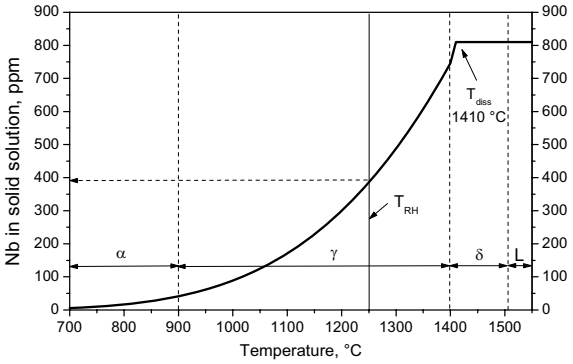

Figure 10. Equilibrium solute Nb content *vs.* temperature.

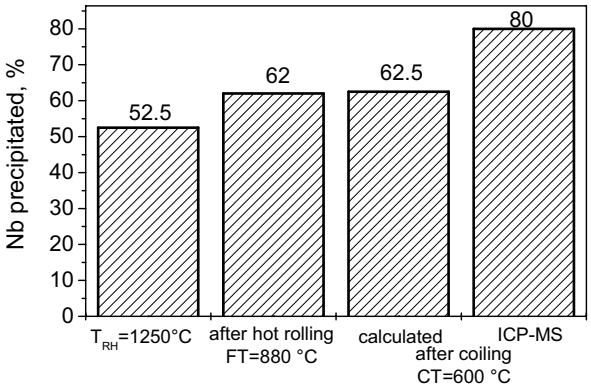

Figure 11. Fraction of Nb precipitated during hot rolling of micro-alloyed TRIP steel.

The dissolution of NbC in the Nb micro-alloyed TRIP steel is clearly not complete during the reheating: 52.5 % of Nb was still present as precipitates at this stage. The model calculations also show that 62 % of Nb precipitated during the hot rolling, i.e. the model predicts that the NbC precipitation for the Nb micro-alloyed TRIP steel are expected to take place during the hot rolling. According to model calculations, almost no additional precipitation of NbC occurred during coiling at 600 °C. The amount Nb precipitated was 62.5 % and the diameter of NbC was 20 nm. The experimental ICP-MS results for precipitated Nb after a coiling simulation gave a value of 80 %. These experimental ICP-MS results, were used for the further model calculations of the precipitation during intercritical annealing.

Annealing

The calculated volume fractions of NbC in ferrite and austenite during the IA and the IBT are shown in Figure 12. Below the A_{e1} temperature, the calculation was only done for the ferrite. Above the A_{e1} temperature, the volume fractions of ferrite and austenite were assumed to be constant and equal to the equilibrium phase fractions. The model calculations showed that NbC precipitates tend to coarsen during the IA. The precipitation already started during the heating prior the IA. A lower amount of precipitate volume fraction of NbC was achieved due to their higher solubility product and the lower diffusivity of Nb in austenite compared to ferrite. No further NbC precipitation occurs during the IBT due to a very low diffusivity of Nb in both ferrite and austenite at 460 °C. The calculated amount of precipitated Nb during full processing of the Nb micro-alloyed TRIP steel was 74 vol. %. According to the ICP-MS measurement, no Nb remained in solid solution after the annealing stage. The calculated diameters of the NbC are 26 nm in the ferrite and 20.1 nm in the austenite, respectively.

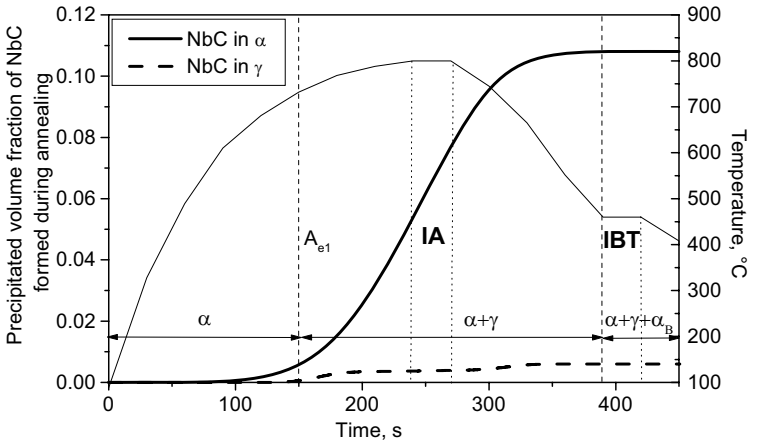

Figure 12. Calculated NbC volume fractions in ferrite, austenite and bainite during IA and IBT.

The lower precipitate volume fractions predicted by the model may be caused by the fact that the model does not take into account a change of the volume fraction of the ferrite and the austenite during the heating. Above the A_{e1} temperature, the equilibrium volume fraction was used for the calculation. This ferrite volume fraction is therefore lower than the actual one during the ferrite into austenite transformation. As ferrite provokes more rapid NbC precipitation compared to austenite, the lower amount of the ferrite, used for the calculation, accounts for a lower precipitated volume fraction compared to the actual situation. Moreover, the calculation used an equilibrium amount of ferrite (60 %) and austenite during IA, which might differ from the actual situation when the equilibrium conditions are not reached. Figure 13 shows NbC precipitates in the ferrite after the full processing of the Nb micro-alloyed TRIP steel. The precipitate size of NbC is 30 ± 1.5 nm in ferrite and 19 ± 1 nm in austenite. This is in agreement with the model calculation, which predicted that the NbC particles were larger in diameter in ferrite than in austenite. As deduced from the model calculations, a significant part of the NbC precipitates was not fully dissolved after the reheating. The pre-existing precipitates tend to grow during the processing of the Nb micro-alloyed TRIP steel; this may limit the strengthening potential of NbC.

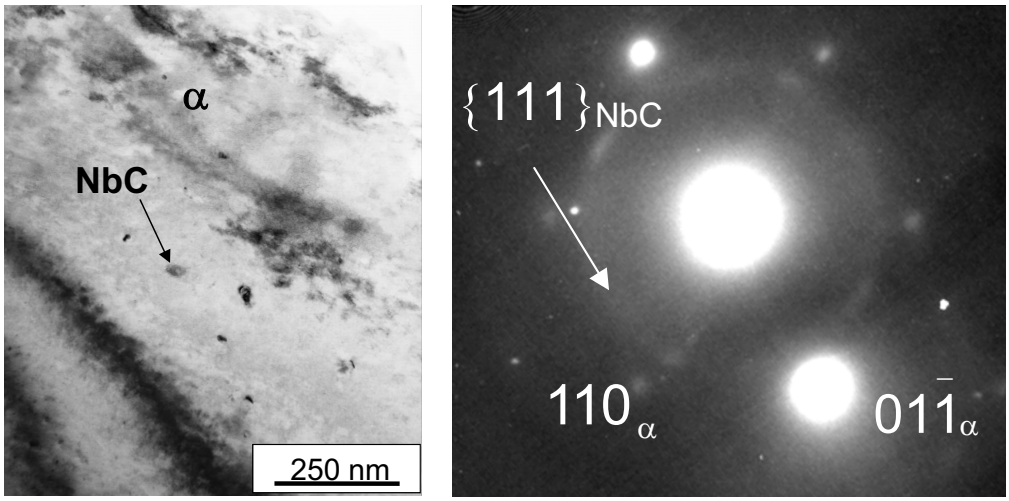

Figure 13. TEM micrograph of NbC precipitates in ferrite in the Nb micro-alloyed TRIP steel.

Microstructures

The microstructure of the reference and the Nb micro-alloyed TRIP steels etched in LePera reagent is shown in Figure 14. In these images, the ferrite appears as grey. The dark bainitic phase generally surrounds the bright phases, which are either retained austenite and/or martensite. In general, the Nb micro-alloyed TRIP steel had a finer microstructure than the reference material. The finer ferrite grains in the Nb micro-alloyed TRIP steel were also surrounded by very fine bainite and retained austenite particles.

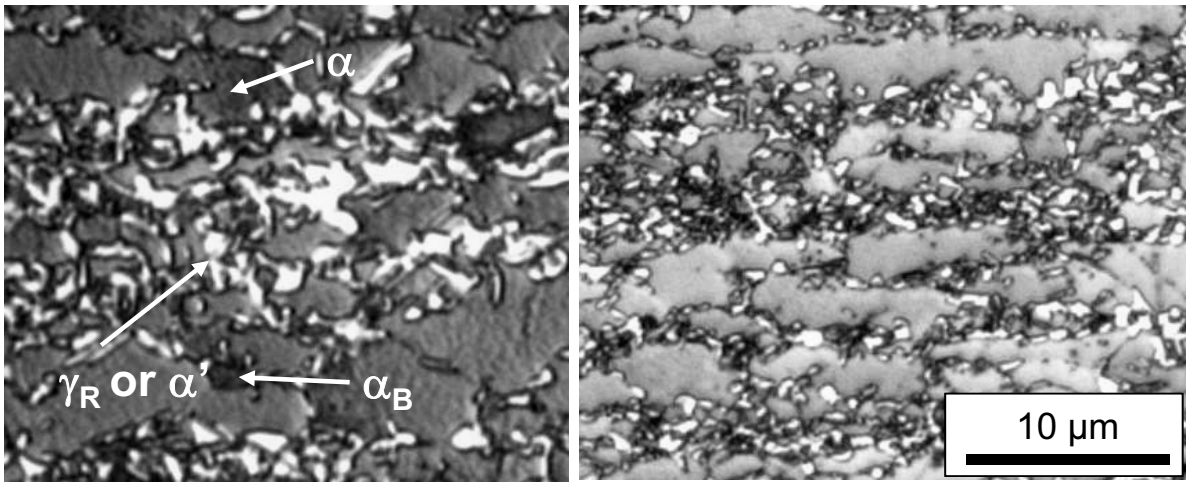

Figure 14. Microstructure refinement due to the addition of Nb: reference TRIP steel (left), Nb micro-alloyed TRIP steel (right). T_{IA} = 800 °C, T_{IBT} = 460 °C.

The volume fractions of the phases present in the TRIP steels, measured by image analysis, are shown in Table II.

Table II. Volume percentage of the phases in the TRIP steels.

	Ferrite	**Bainite**	**Retained austenite/martensite**
Reference	67.9 ± 0.6	15.2 ± 1.3	16.9 ± 0.3
Nb micro-alloyed	69.2 ± 2.5	17.3 ± 1.3	13.5 ± 0.2

Both steels had a similar volume fraction of the ferrite (~ 67 %) while the Nb micro-alloyed TRIP steel had a slightly higher amount of the bainite and a lower amount of retained austenite/martensite particles compared to the reference TRIP steel. The volume fraction of the bainite present in the Nb micro-alloyed TRIP steel was 17.3 ± 3.0 %. The reference TRIP steel had 15.2 ± 1.3 % of bainite. The Nb micro-alloyed TRIP steel had 13.5 ± 0.2 % of M/A particles while the volume fraction of these particles in the reference TRIP steel was 16.9 ± 0.3 %. The grain sizes of ferrite and retained austenite, obtained from LePera and double-etching micrographs, are listed Table III.

Table III. The grain size of the ferrite and retained austenite.

	Ferrite grain size, μm	Retained austenite grain size, μm
Reference	3.4 ± 0.6	1.4 ± 0.1
Nb micro-alloyed	2.7 ± 0.8	1.1 ± 0.1

The ferrite grain size of the reference TRIP steel was 3.4 ± 0.6 μm. The average ferrite grain size in the case of the Nb micro-alloyed TRIP steel was smaller; 2.7 ± 0.8 %. The retained austenite was also refined in the case of the Nb micro-alloyed TRIP steel compared to the reference TRIP

steel. The grain size of the retained austenite in the Nb micro-alloyed TRIP steel is 1.1 ± 0.1 μm while the grain size of the retained austenite measured for the reference TRIP steel is 1.4 ± 0.1 μm.

Characterization of retained austenite

Figure 15 reviews the XRD determination of the volume fraction and the C content of retained austenite. It can be seen that the Nb micro-alloyed TRIP steel had a lower volume fraction of retained austenite. The C content of the retained austenite is also lower for the Nb micro-alloyed TRIP steel compared to the reference material. As Nb effectively combines with C to form NbC, this may explain the lower C content found in the retained austenite of the Nb micro-alloyed TRIP steel. As no NbC precipitation occurs during the bainitic transformation, this implies that austenite in the Nb micro-alloyed TRIP steel must already have a lower C content during the IA. Table IV shows that a very similar volume fraction of ferrite was achieved for both TRIP steels. As no supplementary formation of 'new' pro-eutectoid ferrite is expected, it can be assumed that a very similar amount of the austenite was achieved at the end of the IA. The lower C content of the intercritical austenite causes a shift of the bainite start curve to shorter times, which means that a larger amount of bainite and a lower amount of retained austenite is obtained in the case of the Nb micro-alloyed TRIP steel.

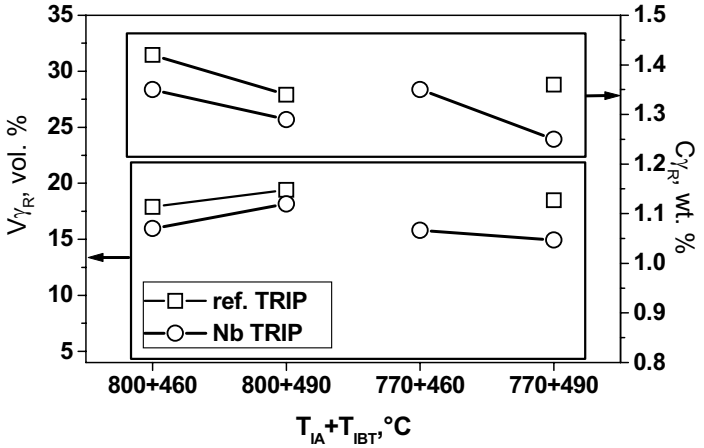

Figure 15. XRD results of the volume fraction and the C content of the retained austenite.

Stability of retained austenite

The stability of retained austenite against the mechanically induced martensite transformation can be characterized by the M_s^{σ} temperature determined by SS-TV-TT method. The M_s^{σ} temperature is temperature at which the transition from continuous to discontinuous yielding occurs. At temperatures lower than M_s^{σ}, the stability of retained austenite decreases and stress-assisted martensite formation proceeds prior to the yielding of retained austenite. The extensive yield point elongation (YPE) occurs on the stress-strain curves as a consequence of the volume expansion associated with the stress-assisted martensitic transformation. At the temperatures higher than M_s^{σ}, retained austenite is stable against the stress-assisted martensite transformation and the strain-induced martensite transformation will proceed by applying a larger plastic deformation than that obtained at the beginning of straining. The results of the SS-TV-TT in a temperature interval from 30 °C to 12 °C for the investigated TRIP steels are shown in Figure 16. The results show that the M_s^{σ} temperature is situated at 18 °C ± 2 °C for both investigated TRIP steels. The M_s^{σ} temperature is below room temperature and the SIMT will therefore proceed at room temperature, which implies well-adjusted retained austenite stability. The same

M_s^{σ} temperature for both investigated TRIP steels means that the retained austenite stability is not influenced by the addition of the micro-alloying elements.

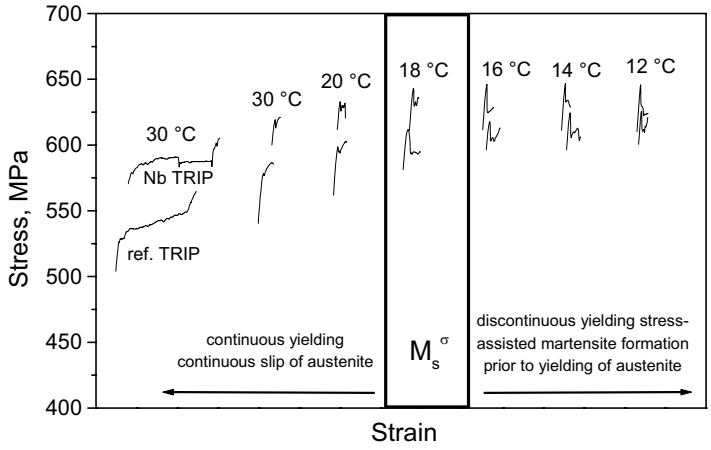

Figure 16. SS-TV-TT M_s^{σ} temperature determination in the range of 30°C-12 °C.

Kinetics of SIMT

The kinetics of SIMT is evaluated using the Olson and Cohen model. The model contains three physically meaningful parameters α, β and n. In this model, the intersections of shear bands are considered to act as effective nucleation sites for the SIMT as the regions of a localization of plastic deformation. These shear bands can be mechanical twins, stacking faults and ε-martensite plates. Olson and Cohen proposed the following equation for $f_{\alpha'}$, the volume fraction of strain-induced martensite:

$$f_{\alpha'} = \frac{V_{\alpha'}}{V_{\gamma_0}} = 1 - exp\left(-\beta \cdot \left[1 - exp(-\alpha\varepsilon)\right]^n\right)$$

where α is a strain-independent constant representing the rate of shear band formation, β is a temperature-dependent parameter, related to the probability that shear band intersections lead to the formation of α' nuclei and n represents a coefficient related to the orientation of the shear bands. The value of n is close to 2 in the case of TRIP steels. A value of $n = 2$ corresponds to a random orientation of the shear band intersections. In order to reduce a number of fitting parameters, a value of $n = 2$ was also used in the present work. Figure 17 and 18 give the fitting of the experimental data on the kinetics of the SIMT using the Olson-Cohen model. The curves had the expected sigmoidal true strain dependence, reaching a SIMT saturation value that decreases at increasing temperature. This implies that in both cases the transformation was never completed even for the lowest testing temperature. The kinetics of the SIMT was slowed down and the saturation values were lower with increasing temperature for both TRIP steels tested. The transformation behavior of the retained austenite was similar for both materials. To illustrate this, Figure 19 shows the kinetics of the SIMT for both TRIP steels at a temperature of 40 °C. The transformation curves are very close to each other.

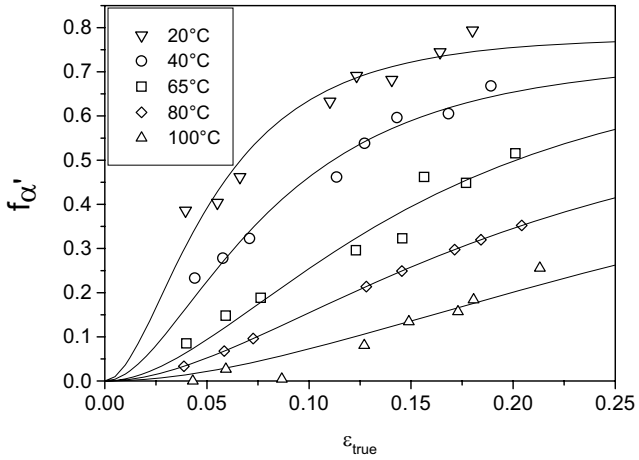

Figure 17. Transformation rate for the reference TRIP steel.

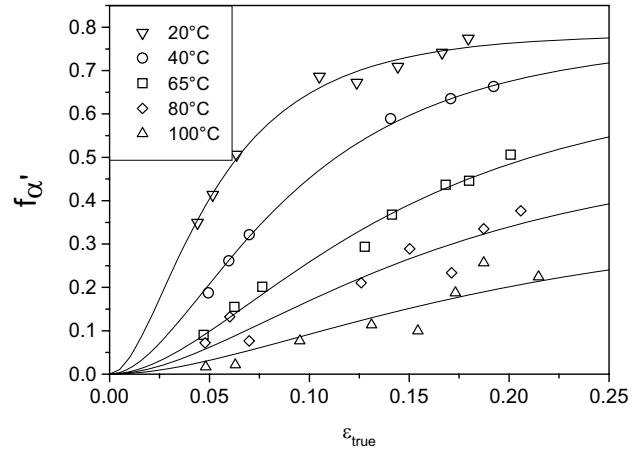

Figure 18. Transformation rate for Nb micro-alloyed TRIP steel.

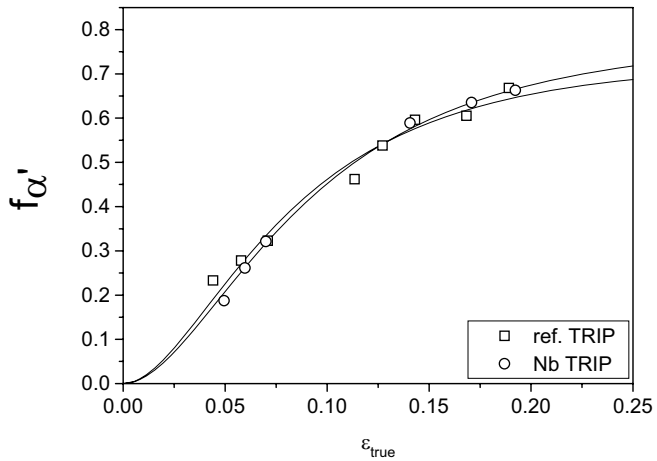

Figure 19. Kinetics of the SIMT for the investigated TRIP steels at 40°C.

Mechanical properties

Figure 20 and 21 show yield strength, tensile strength and total elongation of both TRIP steels investigated for different combinations of T_{IA} and T_{IBT}. The Nb micro-alloyed TRIP steel reached slightly higher yield and tensile strength levels compared to the reference TRIP steel. The addition of Nb also caused a slight decrease of the total elongation. An IA at a lower temperature results in a lower tensile strength. This phenomenon might be explained by a higher amount of high strength bainite formed after IBT as the consequence of the higher amount of intercritical

austenite present at a higher T_{IA}. A higher T_{IBT} resulted in a decrease of yield strength, tensile strength and total elongation. This can be explained in terms of the lower retained austenite stability due to its lower C content at a higher T_{IBT} causing its destabilization.

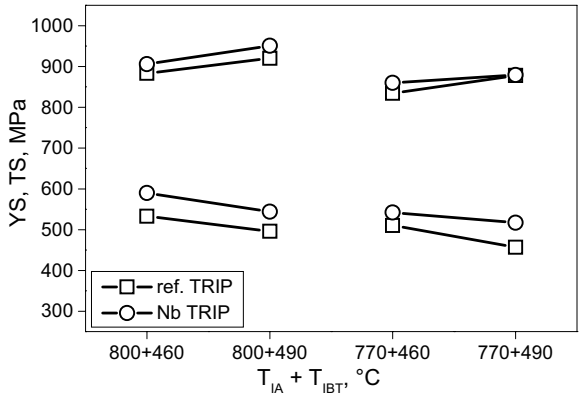

Figure 20. Yield and tensile strength for different combinations of T_{IA} and T_{IBT}.

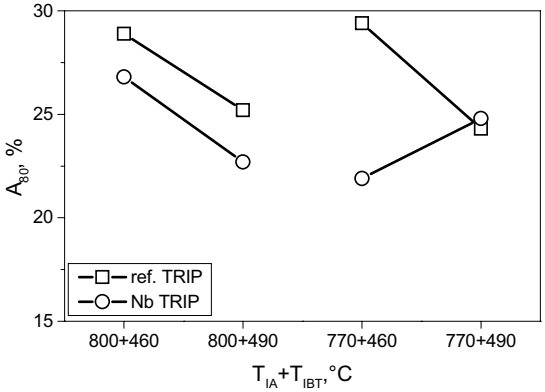

Figure 21. Total elongation for different combinations of T_{IA} and T_{IBT}.

Discussion

Stability of retained austenite and kinetics of SIMT

Table IV and Figure 22 summarize the influence of the various stabilization parameters on the stability of retained austenite and the kinetics of the SIMT in the case of the Nb micro-alloyed TRIP steel. The influence of the microalloying on the stabilization parameters is as follows:
The C content: C effectively combines with the micro-alloying elements to form carbides. Therefore a lower C content of the retained austenite is observed in the case of the Nb micro-alloyed TRIP steel compared to the reference material. The lower C content of the retained austenite in the Nb micro-alloyed TRIP steel acts as destabilizing factor.

The size of retained austenite: A lower grain size of the retained austenite was observed in the case of the Nb micro-alloyed TRIP steel compared to the reference material. The lower grain size is the main factor, which stabilizes the retained austenite in the micro-alloyed TRIP steels due to the decrease of the potential nucleation sites for the SIMT.

Yield strength of retained austenite: The smaller grain size and precipitation strengthening increase the yield strength of retained austenite. This mechanically stabilizes retained austenite and the kinetics of the SIMT is also decreased due to the decrease of the autocatalytic effect. On

the other hand, an increase of the yield strength destabilizes the retained austenite as one of the factors increasing the M_s^{σ} temperature.

Hardness of matrix: Due to the precipitation strengthening of the ferritic matrix the resulting hydrostatic pressure increases, causing an additional stabilization of retained austenite.
Morphology and distribution of retained austenite in microstructure: The morphology of the retained austenite is not significantly influenced by the addition of Nb.

ISFE: The ISFE is not influenced by the addition of Nb as it is entirely combined in precipitates.

The stability of retained austenite is directly related to the kinetics of the SIMT. A higher stability of retained austenite means that retained austenite is more resistant against the SIMT during plastic deformation of TRIP steel and therefore the kinetics of the SIMT is slowed down and *vice versa*. As can be seen, the addition of the micro-alloying elements influences a number of stabilization factors, which stabilize or destabilize retained austenite. It seems from the M_s^{σ} temperature determination and the interrupted testing method followed by V_{γ} measurements that the overall stability of retained austenite and the kinetics of the SIMT are however not significantly influenced by the addition of micro-alloying elements. It has to be pointed out that the additional information has to be gained to determine the actual amount of micro-strain present in retained austenite during straining of the investigated TRIP steels.

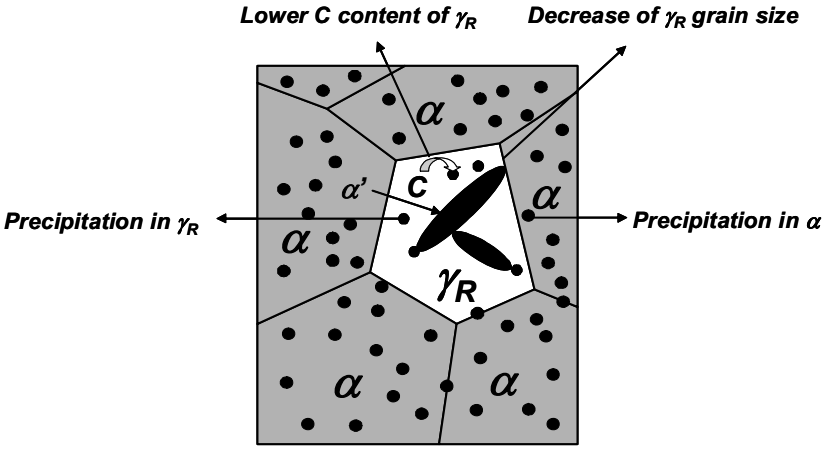

Figure 22. Influence of the micro-alloying elements on the factors determining the stability of retained austenite in a micro-alloyed TRIP steel.

Figure 23 shows the results of the model calculation of the M_s^{σ} temperature as the function of the mean radius of the retained austenite particles for both TRIP steels. In the case of the micro-alloyed TRIP steels, the M_s^{σ} temperature increased due to the precipitation strengthening, grain refinement and a lower C content of retained austenite. A smaller grain size could however also result in a decrease the M_s^{σ} temperature, as it causes the stabilization of the retained austenite, due to the decrease of the potential nucleation sites for the strain-induced martensite transformation. The stabilization effect by refinement of the retained austenite seems more pronounced that its destabilization effect due to the increase of the strength of the austenite. The SS-TV-TT showed that the M_s^{σ} temperature is close to 18 °C for both TRIP steels. The model calculations showed that to achieve the same M_s^{σ} temperature, the grain size of the retained austenite had to be smaller in the case of the Nb micro-alloyed TRIP steel compared to the reference material as the consequence of a higher yield strength of the Nb micro-alloyed TRIP steel compared to the reference material. These observations were also confirmed by the

measurement of the grain size of the retained austenite Table III where the Nb micro-alloyed TRIP steel had a lower grain size of the retained austenite than the reference material.

Table IV. Effect of the addition of microalloying on the factors influencing the stability of retained austenite and the kinetics of the SIMT.

Factor	**Influence**	**Stability of γ_R**	**Kinetics of SIMT**
C content of γ_R	Decreases	Destabilization	Acceleration
Grain size of γ_R	Decreases	Stabilization	Slow down
Yield strength of γ_R	Increases	Stabilization/ Destabilization	Acceleration/Slow down
Hardness of matrix	Increases	Stabilization	Slow down
ISFE in γ_R	Not influenced	No effect	No effect
Morphology of γ_R	Not influenced	No effect	No effect
Micro-strain in γ_R	Not investigated	No effect	Unknown

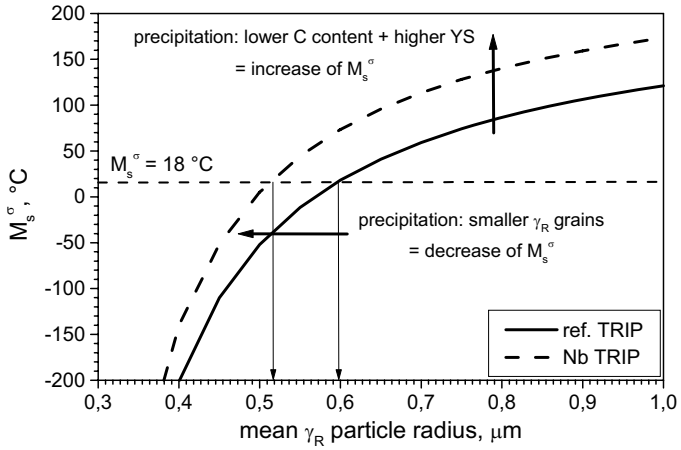

Figure 23. Application of the model predicting the M_s^σ temperature behavior to the micro-alloyed TRIP steels.

Mechanical properties

In Figure 24 it can be seen that the strengthening contribution due to the addition of Nb is limited and that a tensile strength of 1 GPa is not achieved. This is mainly due to the fact that the complete dissolution of NbC was not achieved during the reheating stage. This resulted in a relatively large NbC precipitate diameter (D_{NbC} = 30 nm), which limited the ability of NbC precipitates to pin the austenite and ferrite grain boundaries during the processing of the Nb micro-alloyed TRIP steel. The precipitation strengthening of the coarse NbC particles was also limited. It is clear that in order to use Nb micro-alloying to obtain a 1 GPa TRIP steel, the Nb content must be lowered. Moreover, the addition of V in the Nb micro-alloyed TRIP steel can significantly increase the amount of Nb in solid solution after reheating as schematically explained in Figure 25. This is due to the very high solubility of VC in austenite. As the carbides of micro-alloying elements have the mutual solubility, the dissolution temperature of NbC can be significantly lowered by V addition due to the formation of (Nb,V)C.

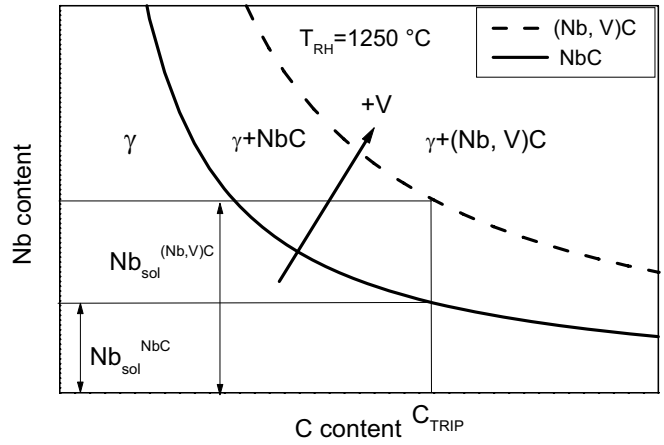

Figure 24. Schematic showing that the addition of V may result in an increase of solute Nb.

Furthermore, the temperature range of (Nb, V)C precipitation can be controlled during both hot rolling and during annealing by the addition of V to the Nb micro-alloyed TRIP steel, Figure 25. The maximal precipitation rate of (Nb, V)C occurs at lower temperatures compared to NbC.

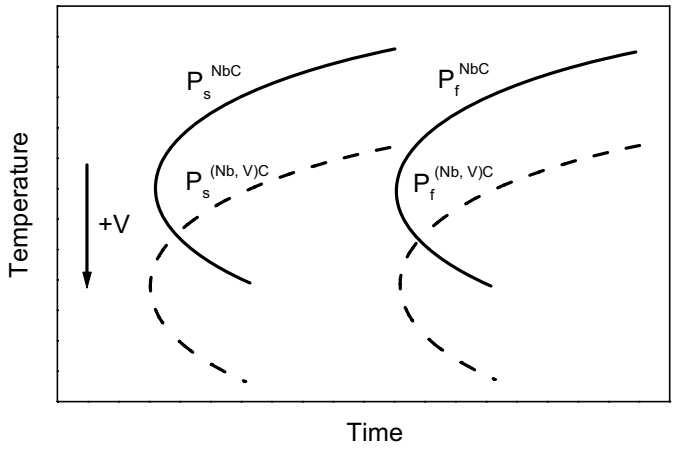

Figure 25. Schematic precipitation time temperature (PTT) diagram showing the effect of V-additions on the temperature range for carbide precipitation in a Nb micro-alloyed TRIP steel.

Conclusions

The main conclusions of the present investigation are as follows:

The addition of the Nb refined the final microstructure of low- alloy TRIP steels. Furthermore, the addition of Nb also resulted in a slightly lower volume fraction and C content of retained austenite than in the reference TRIP steel.

Although the addition of Nb influenced a number of stabilization factors, it could appear from the M_s^{σ} temperature determination that the overall stability of retained austenite in the micro-alloyed TRIP steels is not significantly influenced. The kinetics of SIMT were also not influenced.

Using the Nb content of the present work, a 1 GPa micro-alloyed TRIP steel was not achieved due to the incomplete NbC re-dissolution during the reheating step. In order to use Nb micro-alloying to obtain a 1 GPa TRIP steel, the solute Nb content must be increased. The addition of V in the Nb micro-alloyed TRIP steel could significantly increase the amount of Nb in solid solution after reheating and lower the region of the maximal precipitation during hot rolling, which might further increase the strength of the Nb micro-alloyed TRIP steel.

References

1. G. Wassermann, Arch. Eisenhüttenwes., vol. 10, 1937, 321
2. V.F. Zackay, E.R. Parker, D. Fahr and R. Bush, Trans. ASM, vol. 60, 1967, 252
3. O.Matsumura, Y.Sakuma, H.Takechi, Trans. ISIJ, vol.27, 1987, 570
4. Y.Sakuma, O.Matsumura, H.Takechi, Metall. Trans. A, vol.22A, 1991, 489
5. O.Matsumura, Y.Sakuma, H.Takechi, Trans. ISIJ, vol.32, 1992, 1014
6. O.Matsumura, Y.Sakuma, H.Takechi, Scripta Metall., vol.21, 1987, 1301
7. B.C.De Cooman, Current Opinion in Solid State and Materials Science, 2004, No. 8, 285
8. J. Mahieu, S. Claessens, B.C. De Cooman, Metall. Mater. Trans. A, vol.32A, 2001, 2905
9. M. De Meyer, J. Mahieu and B.C.De Cooman, Mater. Sci. Technol., vol.18, 2002, 1121
10. M. De Meyer, PhD. Thesis, "Transformations and Mechanical Properties of Cold Rolled and Intercritically Annealed CMnAlSi TRIP Steels", Ghent University, July 2001.
11. J. Maki, J. Mahieu, B.C. De Cooman, S. Claessens, Mater. Sci. Technol., vol .19, 2003, 121
12. L. Barbé, L. Tosal-Martinez, B.C. De Cooman, Proc. Int. Conf. on TRIP High Strength Ferrous Alloys, GRIPS, Ghent, Belgium, 2002, 147
13. J. Ohlert, W. Bleck and K. Hulka, Proc. Int. Conf. on TRIP High Strength Ferrous Alloys, GRIPS, Ghent, Belgium, 2002, 205
14. W. Bleck, K. Hulka, P. Papamentellos, Mater. Sci. Forum, vol. 284-6, 1998, 327
15. S. Jiao, F. Hassani, R. Donaberger, E. Essadiqi, S. Yue, ISIJ Int., vol. 42, 2002, 299
16. D.Q. Bai, A. Di Chiro, S. Yue, Mater. Sci. Forum, vol. 284-6, 1998, 253
17. Zarei Hanzaki, P.D. Hodgson, E.V. Pereloma, Proc. High-Strength Steels for Automotive Symposium, ISS, Warrendale, PA, USA, 1994, 53
18. I.B. Timokhina, P.D. Hodgson, E.V. Pereloma, Proc. Int. Conf. on TRIP High Strength Ferrous Alloys, GRIPS, Ghent, Belgium, 2002, 153
19. M. Onink, C.M. Brakman, F.D. Tichelaar, E.J. Mittemeijer, S. Van Der Zwaag, J.H. Root and N.B. Konyer, Scripta Metall. et Mater., vol. 29, 1993, 1011